AIAA JOURNAL
Vol. 34, No. 1, January 1996

Three-Dimensional Unstructured Viscous Grids by the Advancing-Layers Method

Shahyar Pirzadeh*
ViGYAN, Inc., Hampton, Virginia 23681

A method is presented for generating three-dimensional viscous unstructured grids on complex configurations. The approach stems from a natural extension of the advancing-layers method (ALM) that has been successfully applied to two-dimensional problems in prior work. High-aspect-ratio tetrahedral cells are constructed in viscous dominated flow regions by the ALM, with the remaining isotropic cells generated by the conventional advancing-front method. Relying on a totally unstructured grid-generation strategy, the method benefits from a high degree of flexibility and automation required for generating grids around complex geometries. Sample three-dimensional grids around complex configurations are presented to show the capability of the method.

Introduction

UNSTRUCTURED grid methodology has demonstrated considerable success in computational fluid dynamics (CFD) mainly due to its inherent flexibility for discretization of geometrically complex domains. The growing number of new techniques and publications imply the importance and increased interest in this class of grids. A thorough survey of the subject is given in Ref. 1. However, despite their remarkable effectiveness in computation of complex inviscid flow fields, unstructured grids have yet to provide for the routine computation of the Navier–Stokes equations in three dimensions. The lack of a robust unstructured grid strategy for generating highly stretched cells has been a major obstacle to applying such methodology to complex three-dimensional viscous-flow problems.

Among the numerous references on the unstructured grid methodology in the literature, there are only a few that discuss the problem of three-dimensional viscous flow on unstructured grids. Notable among the references that address unstructured viscous grid generation are those cited in Refs. 2–10. Although most of the reported techniques have provided appropriate results for the specific applications shown, many lack the desired generality, flexibility, efficiency, automation, and robustness.

Semiunstructured techniques, for example, retain some of the limitations of structured grid-generation methods that impair the required flexibility and robustness of the method to handle arbitrary three-dimensional complex configurations. Prismatic grids are efficient in terms of computer memory requirement and are effective as long as the configuration under consideration is relatively simple. For geometrically complex domains, this class of grid-generation techniques requires sophisticated schemes, to ensure the integrity of generated grids, which makes the method computationally intensive.[3] Alternatively, prisms have been coupled with more flexible grids (e.g., tetrahedral) to form hybrid grids.[5] This type of grid requires a special flow solution strategy to treat different cell types in the field. Furthermore, to form a one-to-one connection between the prismatic and tetrahedral cells, an identical number of prism layers should be maintained globally to obscure the quadrilateral faces of prisms that obviously do not match with triangular faces of tetrahedral cells. This may limit the extent and flexibility of the prismatic portion of hybrid grids and, thus, reduce the capability of the method for complex problems. Realistic configurations involving sharp edges, integrated components, gaps between close surfaces, etc., are examples of such complexities that require extra careful attention and enhanced capabilities that the existing semiunstructured techniques may lack.

Received Aug. 8, 1994; revision received Aug. 1, 1995; accepted for publication Aug. 1, 1995.

*Senior Research Engineer, Computational Aerodynamics Division, 30 Research Drive. Senior Member AIAA.

This paper presents an alternate approach to the problem of viscous unstructured grid generation. A new method for generation of highly stretched triangular grids has been recently introduced and successfully applied to two-dimensional problems.[6,10] The approach, referred to as the advancing-layers method (ALM), is based entirely on a modified advancing-front technique and benefits from the generality and flexibility of the conventional advancing-front-based Euler grid generators. Being based on an unstructured grid strategy, the method alleviates the structural limitations of many existing techniques while maintaining a certain degree of grid structure (orthogonality) in the viscous dominated flow region. The present approach generates mono-type tetrahedral grids throughout the computational domains as opposed to hybrid grids. The method has resulted in excellent triangular grids as demonstrated in Refs. 6 and 10. The extension of the methodology to three-dimensional problems is presented in this paper.

Approach

Similar to the two-dimensional version of the method, the present approach is divided into three separate stages: 1) surface grid generation, 2) construction of high-aspect-ratio cells in the viscous region, and 3) generation of regular (isotropic) cells in the inviscid-flow region. Steps 1 and 3 utilize established methodology encompassed in an existing advancing-front inviscid grid-generation code VGRID.[11,12] The second step is performed independently by the ALM to reduce the overall complexity of the process. Although the generation of grid is divided into separate stages with the present approach, the entire process is performed in a single run with automatic transition from one stage to another.

Basic Concept

The main features of the advancing-layers techniques are similar to those of the conventional advancing-front method (AFM).[11] A volume grid is generated through a marching process in which tetrahedral cells originate from a triangular surface mesh and proceed into the computational domain. In contrast to the conventional method that adds cells in the field in no systematic sequence, the ALM advances one layer of cells at a time to reduce the complexity of producing high-aspect-ratio cells. Cells are formed by connecting new grid points, inserted along predetermined surface vectors, to the corresponding faces on the front. During the process, the integrity of the generated grid is monitored at each step. The layers continue to advance in the field, while growing in thickness, until either 1) opposite fronts approach to within a local cell size or 2) certain grid quality criteria, dictated by a global background grid, are locally satisfied. When the conditions are met on all faces on the front, the process automatically switches from the advancing-layers to the advancing-front mode to generate equilateral cells in the remaining inviscid-flow region. The details of the process are given in Ref. 6.

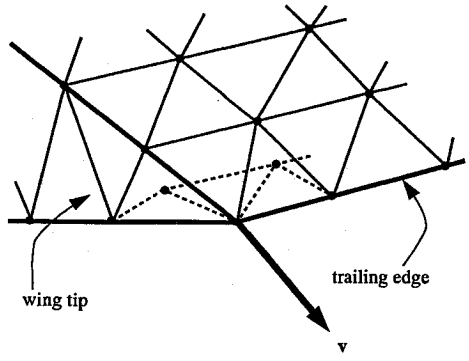

Fig. 1 Surface vector at the tip/trailing-edge corner of a wing.

The basic concept of the original ALM in two dimensions was devised with three-dimensional problems in mind, resulting in a rather straightforward extension of the method to three dimensions. Although most features of the present method are identical to the original version in two dimensions, there are some differences and additional requirements for three-dimensional problems that are discussed in the following sections.

Surface Vectors

A crucial element in the present and many semiunstructured grid methods is the determination of surface vectors along which the grid points are distributed. A necessary condition to prevent formation of negative cells at sharp convex corners/edges is that the surface vectors at mesh points be visible by all triangular faces connected to the corresponding points.[4] Although the computation of vectors is trivial in two dimensions and may be achieved by a simple averaging of the face normals,[6] their calculation becomes more involved in three dimensions and requires careful attention.

In two dimensions, a surface grid point is shared by only two linear faces. The resultant of two adjacent face normals always represents the bisector of the angle between the two faces and satisfies the visibility condition. On the other hand, surface mesh points are linked to an arbitrary number of triangular faces in a three-dimensional unstructured grid. Depending on the local surface contour and triangulation, a simple average of the face normals may violate the visibility condition at sharp convex corners. The situation is shown in Fig. 1 for an example in which a simple resultant vector $\boldsymbol{v}$ at the tip/trailing-edge corner of a wing is inclined downward due to an uneven distribution of triangles on the tip, upper, and lower surfaces of the wing.

An ideal surface vector at a node is one that is equally visible by all of the faces surrounding the node. A method is described in Ref. 4 for the calculation of surface vectors most normal to the faces connected to the corresponding surface grid points. A simpler approach, taken in this work, is based on the observation that a surface vector at a node making equal angles with the surrounding faces is a valid vector, i.e.,

$$\boldsymbol{v}_p \cdot \boldsymbol{n}_f = c; \qquad f = 1, 2, \ldots, F_p \tag{1}$$

where $\boldsymbol{v}_p$ is a surface vector at point p, $\boldsymbol{n}_f$ is the unit normal of the fth face connected to point p, c is a positive constant (visibility constraint), and F_p is the total number of faces surrounding point p. A solution to Eqs. (1) is obtained by an iterative scheme through the following steps.

1) Compute the surface vector $\boldsymbol{v}_p$ by weighted averaging of the face unit normals,

$$\boldsymbol{v}_p^t = \omega \sum_{f=1}^{F_p} w_f^t \boldsymbol{n}_f + (1-\omega)\boldsymbol{v}_p^{t-1} \tag{2}$$

where w_f^t is a weighting function assigned to the fth face at iteration level t, and ω is a relaxation factor. The iterations start with a simple average of the minimum and maximum components of face normals as initial $\boldsymbol{v}_p$ and a value of $1/F_p$ for all w_f.

2) Evaluate the angles that $\boldsymbol{v}_p$ makes with each face normal $\boldsymbol{n}_f$ and their deviations δ_f from the average angle $\bar{\alpha}$.

3) Predict a new weighting function $\tilde{w}_f$ for the next iteration,

$$\tilde{w}_f^{t+1} = w_f^t \left(1 - \frac{\delta_f}{\bar{\alpha}}\right) \tag{3}$$

4) Correct the new weighting function,

$$w_f^{t+1} = \tilde{w}_f^{t+1} + w_f^t \left(1 - \sum_{f=1}^{F_p} \tilde{w}_f^{t+1}\right) \tag{4}$$

5) Continue steps 1–4 until changes in $\boldsymbol{v}_p$ are negligible.

The preceding scheme converges in a few iterations and has consistently produced valid surface vectors for all cases considered thus far. Additional relaxation of the corrected weighting functions [Eq. (4)] improves the rate of convergence for cases with extremely sharp edges. Also for most cases, incorporation of the initial vectors with the final result would offset biased inclinations and produce nearly ideal vectors everywhere.

The surface vectors are next smoothed through a Laplacian-type operation[6] in a few iterations with those along sharp edges held fixed. The vectors are calculated and smoothed once, after a surface mesh is generated, and used throughout the advancing-layers process. To maintain the orthogonality of the vectors near the surfaces, the unsmoothed (orthogonal) vectors can be optionally used for the first layer of cells with the influence of the smoothed vectors increasingly added as the layers advance in the field.

Advancing-Layers Process

The process of advancing layers is performed by successively selecting a triangular face on the front, adding new points along the three predetermined surface vectors that emanate from the vertices of the face, and connecting the new points to the face vertices to generate tetrahedral cells. The distribution of points along vectors is determined by a prescribed stretching function that provides total control over the extent of the cell aspect ratio. During the process, old faces are removed from the list of active faces, and new ones are created and added to the front. Only those faces with all vertices on the same layer (primary faces) are considered active and are selected to form new cells.

As mentioned earlier, generation of grids by the ALM is performed more systematically than that by the conventional AFM. The new procedure requires considerably fewer numbers of floating-point calculations, which has resulted in a substantial improvement in the performance and accuracy of the marching process. Also, to further increase the efficiency of the algorithm, a group of three tetrahedral cells is simultaneously formed on a triangular face at each step. The process, however, introduces an additional requirement that is specific to the ALM in three dimensions. As discussed in Ref. 8, care must be taken to form compatible connectivities among the neighboring groups of cells. In other words, the triangular faces formed on the sides of each cell grouping must match those of the adjacent groups.

In the conventional AFM, proper connectivities are guaranteed by extensive use of a face-cross-check algorithm. The process is, however, time consuming and lacks the desired accuracy and robustness for viscous grids with extremely small spacings. Instead, a simple all-integer algorithm is developed, in this work, to prepare a pattern of compatible connectivities among the cells in the viscous grid layers. Considering a triangular face on the current front (lower level) with a local connectivity 1-2-3 (see Fig. 2) and three corresponding new points 1′, 2′, and 3′ on the next layer (higher level), one can form six possible connectivities for three tetrahedra as shown. The arrows denote the direction of diagonals, connecting a lower to a higher level node, as projected onto the edges of the surface triangles. Associated with each diagonal connectivity is an identifying number (shown in squares), and each group of cells is labeled by a number defining its connectivity type (shown in circles). Note that the numbers for cell connectivities are the sum of the numbers assigned to their corresponding diagonals. The numbers chosen for the diagonals have the property of adding to unique cell numbers. Given a surface triangulation and information regarding the neighboring triangles, the algorithm proceeds by marching through surface triangles in a single pass, assigning appropriate cell connectivity type to each triangle

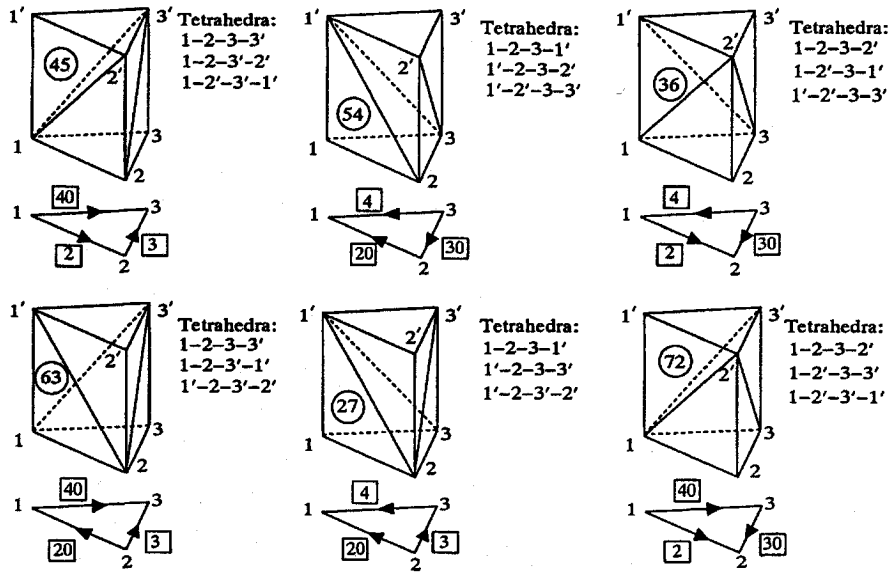

Fig. 2 Different connectivities for a group of three tetrahedral cells formed on a surface triangular face: □, diagonal type and ○, cell connectivity type.

under consideration, and simultaneously adding corresponding diagonal numbers to the (accumulated) cell numbers of the neighboring triangles. Through this simple updating/assigning procedure, the connectivity numbers for cells add to proper values successively, and compatible connectivity types propagate throughout the surface mesh in a systematic manner. A connectivity pattern is prepared once on the surface mesh, before the volume grid generation starts, and is used for all layers of cells to be generated. Figure 3 shows a sample surface patch triangulation along with a connectivity pattern for generation of cell layers on the triangles. The numbers, in this figure, indicate the cell connectivity types given in Fig. 2, and the arrows represent edge connections between two groups of cells as also shown in Fig. 2. The algorithm is efficient, as there are no iterations involved, and has successfully worked for all the cases considered thus far.

The layers continue marching in the field by inserting and connecting new points, according to the predetermined pattern, and forming high-aspect-ratio tetrahedral cells in the viscous dominated regions. The extent by which layers advance is determined by 1) the size, shape, and quality of the cells being formed and 2) the proximity of two approaching fronts.

Even though a background grid does not directly determine the distribution of volume grid in the viscous region, as it does for the generation of isotropic grids,[13] it controls how far layers march in the field. When the grid spacing, determined by the stretching function, locally matches that dictated by the background grid, the front (layer) stops marching in that location. The advancement of layers is also limited by criteria that control the shape and quality of the cells. At sharp corners, for example, where the surface vectors diverge (converge) extensively, cells stretch (shrink) faster than the neighboring cells, and the layers stop progressing earlier than those in other regions. Among the criteria used for this purpose are the actual spacing, face area, and cell skewness, as compared with the corresponding ideal values based on the background grid information. With a common background grid controlling both the advancement of viscous grid layers and the distribution of grid points outside the boundary layer, the transition from a stretched grid, generated by the advancing layers, to an isotropic grid, constructed by the AFM, becomes smooth and gradual.

To prevent two opposite fronts from crossing each other, the position of each new point to be introduced must be checked with respect to the nearby fronts before new cells are formed. As mentioned earlier, a computer-intensive algorithm is used in the conventional AFM to determine whether a new cell actually intersects any face on the existing front. Alternatively, a simple criterion based on a spring analogy was introduced and used in Ref. 6 to monitor the proximity of faces on two different fronts. An extension of that approach to three dimensions is applied in the present work. In this technique, a new grid point is assumed to be fixed in space and connected to the vertices of the face under consideration by tension springs as shown

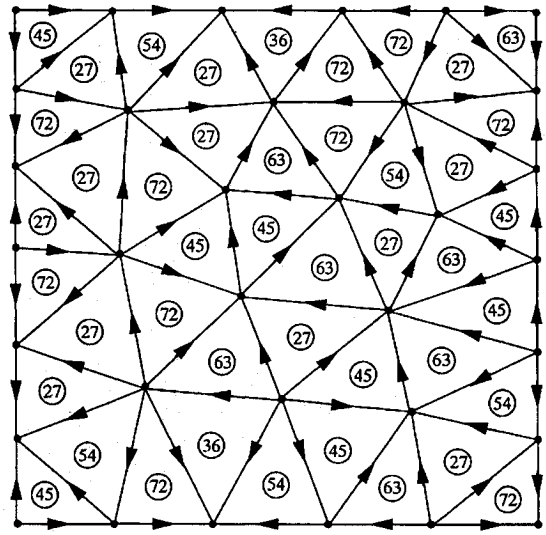

Fig. 3 Connectivity pattern for a sample surface triangulation.

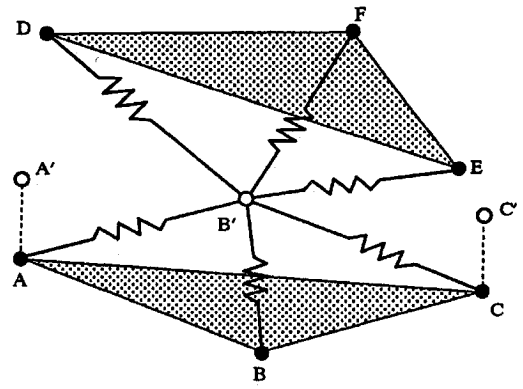

Fig. 4 Detection of front proximity by a spring analogy.

in Fig. 4. The total force exerted on the point is equal to the sum of the tensions of springs that are, in turn, proportional to the spring displacements, i.e.,

$$F_f^p \propto \frac{1}{r_f} \sum_{n=1}^{N} s_n \tag{5}$$

where F_f^p is the total force on point p connected to face f, s_n is the distance by which the nth spring is displaced (stretched) from its neutral length (i.e., the length when the point is positioned at the centroid of the face resulting in zero tension), N is the number of

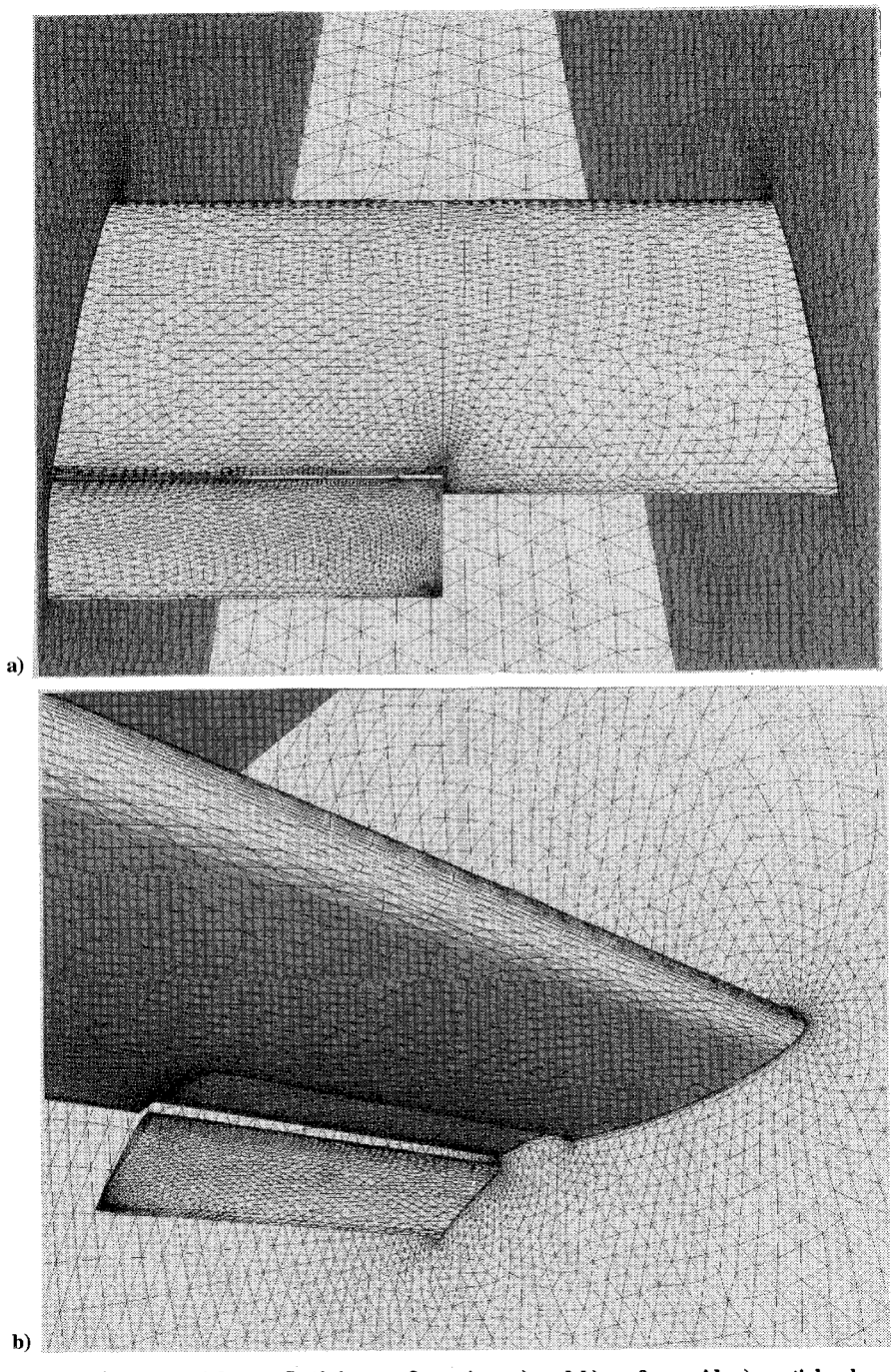

Fig. 5 Tetrahedral viscous grid for a partial-span flap/wing configuration: a) and b) surface grid, c) partial volume grid at final stage of the advancing-layers process, and d) partial volume grid by the AFM.

springs connected to point p (2 in two and 3 in three dimensions), and r_f is a characteristic length (such as the square root of area) for the face f. Forces are calculated separately for the three new points in relation to the face to be removed and also with respect to all other close faces. In Fig. 4, for example, a face under consideration (ABC) is shown connected to one of the three tentative new points (B') that is also connected to a close face DEF by springs. When the maximum of the forces, which the face to be removed exerts on the three new points, becomes greater than the minimum of the forces that all existing close faces exerts on the same new points, the opposing fronts are considered to be too close and, thus, stop advancing. For the example in Fig. 4, the face ABC stops marching, and the three new points A', B', and C' are discarded if

$$\max\left(F^{A'}_{ABC}, F^{B'}_{ABC}, F^{C'}_{ABC}\right) > \min\left(F^{A'}_{DEF}, F^{B'}_{DEF}, F^{C'}_{DEF}, \ldots\right) \quad (6)$$

During the formation of new cells, the spring criterion ensures that no other existing face is close enough to obstruct the cells. In fact, approaching fronts stop advancing before they have a chance to cross each other.

When the spacing, quality, and/or proximity criteria are satisfied on all faces on the front, the process automatically changes mode from the advancing-layers to the conventional AFM to form regular isotropic cells in the rest of the domain.

Results

During the development of the method, grids were generated for a variety of test cases ranging from simple, isolated wings to complex multicomponent configurations. For this paper, two representative complex geometries are presented to demonstrate the capability of the method to negotiate difficult aspects, such as opposing fronts in small gaps, and sharp concave and convex corners.

Partial-Span Flap/Wing

The geometry consists of an unswept wing of aspect ratio 2, mounted between wind-tunnel walls, and a deflected flap extended

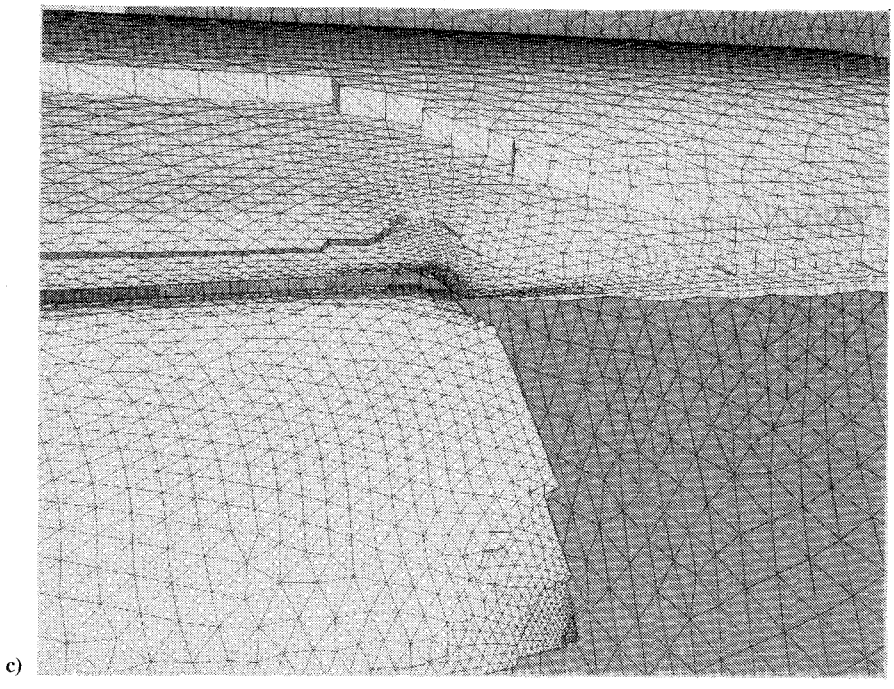

c)

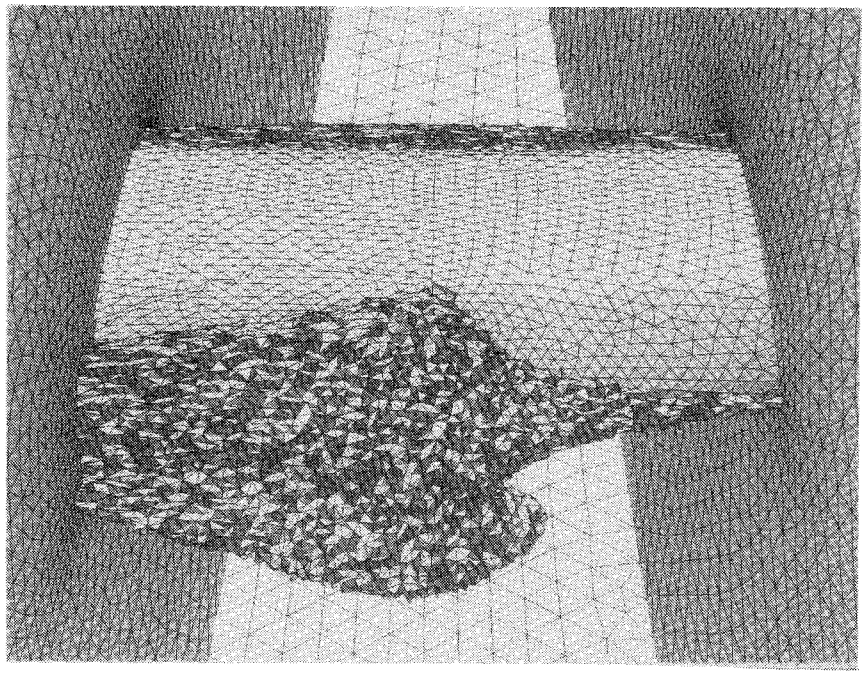

d)

Fig. 5 (continued) Tetrahedral viscous grid for a partial-span flap/wing configuration: a) and b) surface grid, c) partial volume grid at final stage of the advancing-layers process, and d) partial volume grid by the AFM.

to midspan. The configuration contains complex features such as a small gap between the wing and flap and sharp edges. The gap and the overlap sizes between the flap and the wing trailing edge are 0.019 and 0.004 wing chord, respectively. The geometry has been recently tested in the 7 × 10 ft tunnel at NASA Ames Research Center.[14] The generated surface grid, shown in Fig. 5a, contains a total of 21,060 points and 42,120 triangles, including those on the side walls and the outer boundaries. To reduce the number of points and cells, the surface grid is variably stretched in the spanwise direction. A new strategy, currently under development, has been used for generating anisotropic high-aspect-ratio surface and volume grids. The aspect ratio of the surface triangles, in this example, varies from approximately 20 at the leading edge of the wing to 1 at the flap tip and far field with a gradual transition in between. Figure 5b shows a portion of the surface grid at the leading edge of the wing along with the grid on one of the side walls. The viscous grid layers in the boundary layer and their smooth transition to the outer isotropic grid are shown on the side wall.

After the generation of surface grid, the connectivity pattern and surface vectors were constructed in a small fraction of the total grid-generation time. This particular geometry, with extremely sharp edges, has served as a good test case for evaluating the robustness of the surface vector algorithm described earlier. The juncture between the flapped and unflapped wing sections at the trailing edge, for example, has created a geometrically difficult situation involving multiple convex/concave edges converged to a corner point. The angle of the wing trailing edge at this location is only 1.6 deg. The vectors are calculated correctly, all satisfying the visibility criterion.

The viscous portion of the volume grid, generated with the ALM, contains 201,391 points and 1,098,051 tetrahedral cells. The following simple stretching function was used to distribute grid points along surface vectors:

$$\delta_n = \delta_0\left[1 + r_1(1 + r_2)^{n-1}\right]^{n-1} \tag{7}$$

where δ_n is the normal spacing for the nth layer, δ_0 is a prescribed

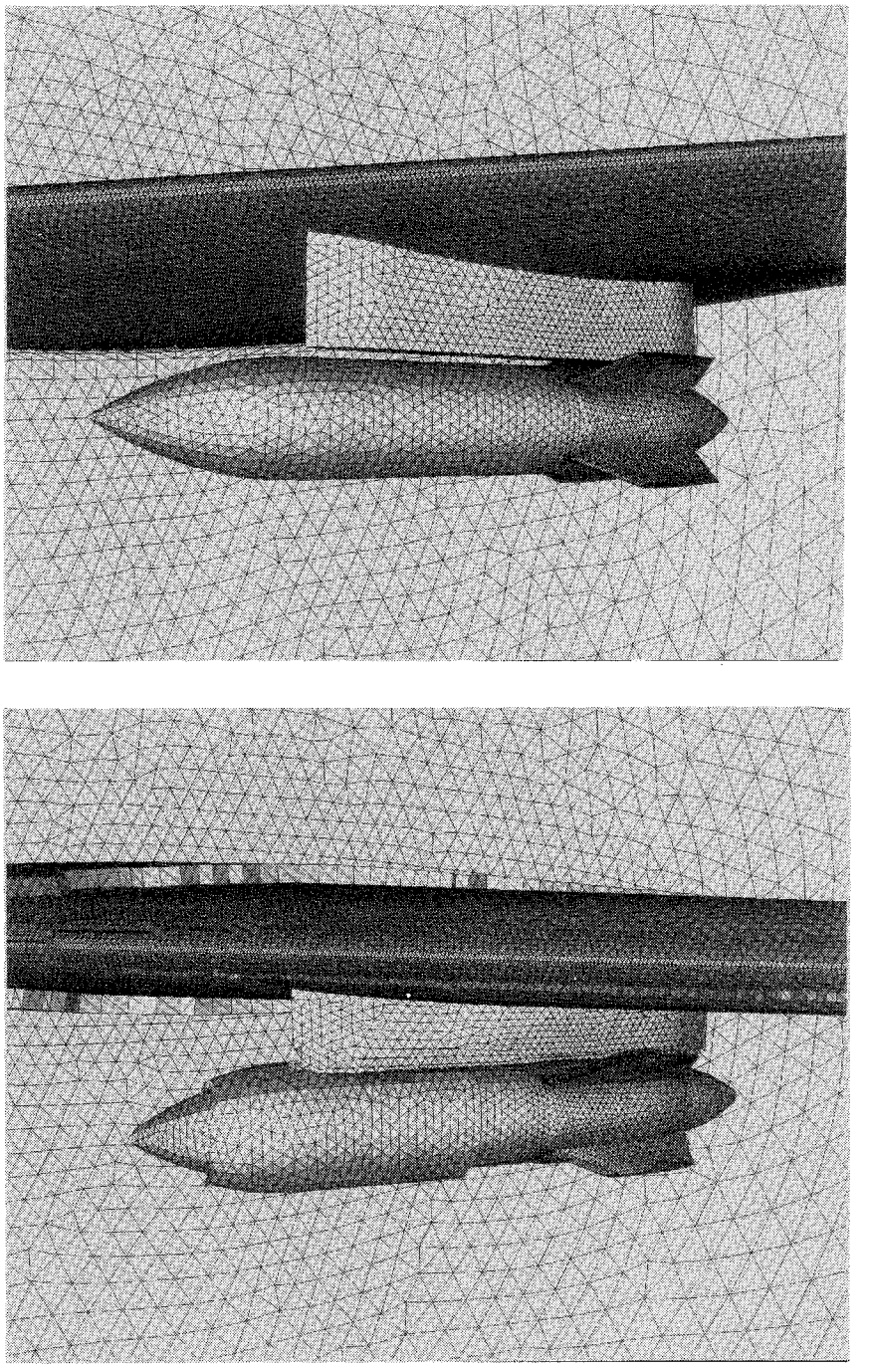

Fig. 6 Tetrahedral viscous grid for a wing/pylon/finned-store configuration: a) surface grid, b) partial volume grid at final stage of the advancing-layers process, and c) a cut through the complete volume grid at midspan.

first layer spacing, and the factors r_1 and r_2 are constants that determine the rate of stretching. For a laminar boundary layer, r_1 and r_2 are set to 0.1–0.2 and 0., respectively. For turbulent flow with a denser distribution of grid points in the viscous sublayer and a faster growth in the rest of the boundary layer, values of 0.04 for r_1 and 0.07 for r_2 have produced satisfactory distributions. A uniform first-layer normal spacing (δ_0) of 10^{-5} main wing chord length has been prescribed for this grid. Figure 5c shows the partial grid at the final stage of the advancing-layers process in which layers of cells have stopped at different levels as monitored by the background grid and the spring criteria.

The rest of the domain is gridded by the more flexible method of advancing front. Figure 5d shows a partial grid in which equilateral tetrahedral cells are formed on the viscous portion of the grid. Since the same background grid monitors the advancement of fronts in both methods, a good compatibility exists between the two procedures resulting in a smooth transition from one grid type to another. The final grid contains a total of 317,860 points and 1,823,387 tetrahedral cells. The entire grid was generated using a Silicon Graphics Indigo^2 workstation with a single R4000(100-MHz) processor in about 80 min. The computation time includes surface and volume grid generation, performed interactively with graphical display of the process at selected intervals, and input/output time.

A turbulent flow computation for this geometry has been performed by Anderson et al.[15] on a similar grid generated with the present method. Good agreement between the experimental and computational results is reported in the paper.

Wing-Pylon-Store

This configuration consists of a clipped delta with a leading-edge sweep angle of 45 deg and a taper ratio of 0.134, a pylon located at the midspan, and a store in the carriage position with four swept-back fins. The complexity of the geometry is characterized by its multiple components, sharp wing trailing edge (4.67 deg), and a very small

c)

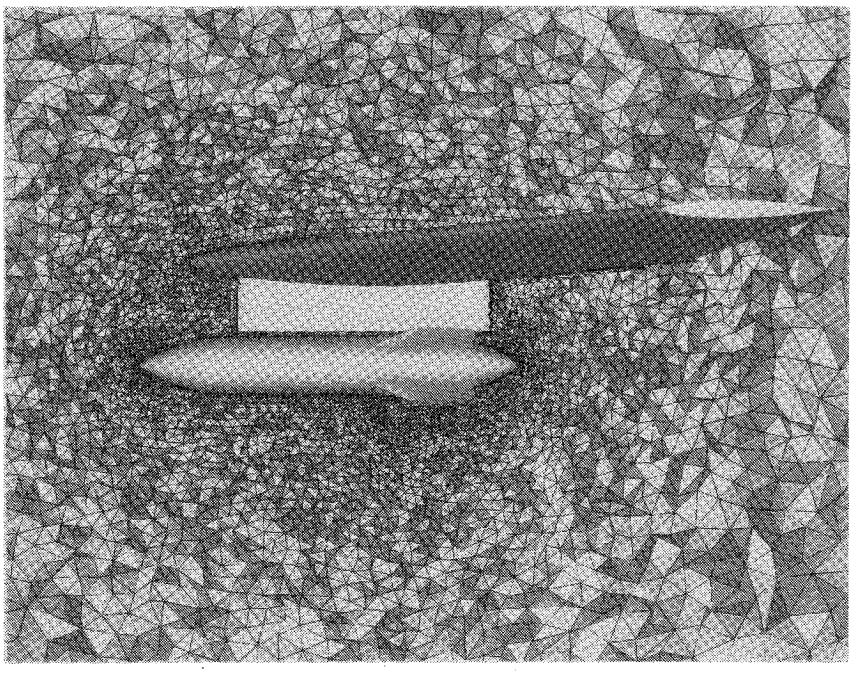

Fig. 6 (continued) Tetrahedral viscous grid for a wing/pylon/finned-store configuration: a) surface grid, b) partial volume grid at final stage of the advancing-layers process, and c) a cut through the complete volume grid at midspan.

gap (0.07 store diameter) between the pylon and the detached store. The geometry specifications along with extensive experimental and computational inviscid flow results are reported in Refs. 16 and 17.

The surface grid, shown in Fig. 6a, contains 24,339 points and 48,670 triangles including the grid on the symmetry plane and the outer boundary. No anisotropic stretching is applied in this grid, resulting in a relatively larger grid size than in the previous case. Figure 6b shows the outermost layers of the volume grid generated with the ALM mode of the grid generator. The grid spacing in the boundary layer is determined from Eq. (7) with a uniform first-layer normal spacing of 6.7×10^{-7} store diameter. The advancement of cell layers has been properly controlled by the spacing and the proximity criteria even in the narrow space between the pylon and store. This example demonstrates the flexibility of the method and the spring criterion for controlling viscous grid layers in close regions of opposite approaching fronts. Figure 6c shows a cut through the complete volume grid at the midspan. The final grid contains 734,207 nodes and 4,300,120 tetrahedra.

Conclusions

A method for the generation of tetrahedral unstructured viscous grid on three-dimensional complex configurations has been introduced. The method benefits from the flexibility and generality of the unstructured grid generation by the advancing-front technique and provides smooth, quasistructured grids in the boundary-layer region without introducing complications usually associated with the structured grid strategies. A simple iterative scheme has been developed to resolve the crucial problem of computing surface vectors in three dimensions. A straightforward front-detection procedure based on the spring analogy and an algorithm for constructing cell connectivities are also developed to eliminate the need for a computationally expensive face-cross-check procedure used in the conventional AFM. The method is efficient, allowing viscous grids be generated on small workstations in a reasonable amount of computational time. The proposed grid strategy along with the conventional advancing-front technique has provided a new, robust approach to the problem of three-dimensional unstructured viscous grid generation.

Acknowledgments

This work was sponsored by NASA Langley Research Center, Contract NAS1-19672, with Neal T. Frink serving as the technical monitor.

References

[1]Thompson, J. F., and Weatherill, N. P., "Aspects of Numerical Grid Generation: Current Science and Art," AIAA Paper 93-3539, Aug. 1993.

[2]Mavriplis, D. J., "Euler and Navier-Stokes Computations for Two-Dimensional Geometries Using Unstructured Meshes," NASA CR-181977, Jan. 1990.

[3]Nakahashi, K., "Optimum Spacing Control of the Marching Grid Generation," AIAA Paper 91-0103, Jan. 1991.

[4]Kallinderis, Y., and Ward, S., "Prismatic Grid Generation with an Efficient Algebraic Method for Aircraft Configurations," AIAA Paper 92-2721, June 1992.

[5]Ward, S., and Kallinderis, Y., "Hybrid Prismatic/Tetrahedral Grid Generation for Complex 3D Geometries," AIAA Paper 93-0669, Jan. 1993.

[6]Pirzadeh, S., "Unstructured Viscous Grid Generation by Advancing Front Method," NASA CR-191449, April 1993.

[7]Müller, J. D., "Proven Angular Bounds and Stretched Triangulations with the Frontal Delaunay Method," AIAA Paper 93-3347, July 1993.

[8]Löhner, R., "Matching Semi-Structured and Unstructured Grids for Navier-Stokes Calculations," AIAA Paper 93-3348, July 1993.

[9]Hassan, O., Probert, E. J., Morgan, K., and Peraire, J., "Line Relaxation Methods for the Solution of 2D and 3D Compressible Flows," AIAA Paper 93-3366, July 1993.

[10]Pirzadeh, S., "Unstructured Viscous Grid Generation by the Advancing Layers Method," *AIAA Journal*, Vol. 32, No. 8, 1994, pp. 1735–1737; see also AIAA Paper 93-3453, Aug. 1993.

[11]Parikh, P., Pirzadeh, S., and Löhner, R., "A Package for 3-D Unstructured Grid Generation, Finite Element Flow Solution and Flow Field Visualization," NASA CR-182090, Sept. 1990.

[12]Pirzadeh, S., "Recent Progress in Unstructured Grid Generation," AIAA Paper 92-0445, Jan. 1992.

[13]Pirzadeh, S., "Structured Background Grids for Generation of Unstructured Grids by Advancing Front Method," *AIAA Journal*, Vol. 31, No. 2, 1993, pp. 257–265.

[14]Storms, B. L., Takahashi, T. T., and Ross, J. C., "Aerodynamic Influence of a Finite-Span Flap on a Simple Wing," Society of Automotive Engineers, SAE Paper 95-1977, Los Angeles, CA, Sept. 1995.

[15]Anderson, W. K., Rausch, D. R., and Bonhaus, D. L., "Implicit/Multigrid Algorithms for Incompressible Turbulent Flows on Unstructured Grids," AIAA Paper 95-1740, June 1995.

[16]Heim, E. R., "CFD Wing/Pylon/Finned Store Mutual Interference Wind Tunnel Experiment," Arnold Engineering Development Center, AEDC-TSR-91-P4, Arnold AFB, TN, Jan. 1991.

[17]Parikh, P., Pirzadeh, S., and Frink, N. T., "Unstructured Grid Solutions to a Wing/Pylon/Store Configuration," *Journal of Aircraft*, Vol. 31, No. 6, 1994, pp. 1291–1296.